Accepted Manuscript

Multiscale approach for identification of transverse isotropic carbon fibre properties and prediction of woven elastic properties using ultrasonic identification

R.D.B. Sevenois, D. Garoz, E. Verboven, S.W.F. Spronk, F.A. Gilabert, M. Kersemans, L. Pyl, W. Van Paepegem

PII: S0266-3538(18)31341-1

DOI: 10.1016/j.compscitech.2018.09.016

Reference: CSTE 7398

To appear in: *Composites Science and Technology*

Received Date: 4 June 2018

Revised Date: 14 September 2018

Accepted Date: 15 September 2018

Please cite this article as: Sevenois RDB, Garoz D, Verboven E, Spronk SWF, Gilabert FA, Kersemans M, Pyl L, Van Paepegem W, Multiscale approach for identification of transverse isotropic carbon fibre properties and prediction of woven elastic properties using ultrasonic identification, *Composites Science and Technology* (2018), doi: https://doi.org/10.1016/j.compscitech.2018.09.016.

Multiscale Approach for Identification of Transverse Isotropic Carbon Fibre Properties and Prediction of Woven Elastic Properties using Ultrasonic Identification

R.D.B. Sevenois[a,b,*], D. Garoz[a,b], E. Verboven[a], S.W.F. Spronk[a,b], F.A. Gilabert[a,b], M. Kersemans[a], L. Pyl[c], W. Van Paepegem[a]

[a] *Department of Materials, Textiles and Chemical Engineering, Faculty of Engineering and Architecture, Ghent University, Tech Lane Ghent Science Park Campus A, Technologiepark Zwijnaarde 903, B-9052 Zwijnaarde, Belgium*
[b] *SIM Program M3Strength, Technologiepark Zwijnaarde 935, B-9052 Zwijnaarde, Belgium*
[c] *Department of Mechanics of Materials and Constructions (MeMC), Faculty of Engineering Sciences, Vrije Universiteit Brussel, Brussels, Belgium*

Abstract

In this work the possibility to reverse engineer the transverse isotropic carbon fibre properties from the 3D homogenized elastic tensor of the UD ply for the prediction of woven ply properties is explored. Ultrasonic insonification is used to measure the propagation velocity of both the longitudinally and transversally polarized bulk waves at various symmetry planes of a unidirectional (UD) Carbon/Epoxy laminate. These velocities and the samples' dimensions and density are combined to obtain the full 3D orthotropic stiffness tensor of the ply. The properties are subsequently used to reverse engineer the stiffness tensor, assumed to be transversely isotropic, of the carbon fibres. To this end, four micro-scale homogenization methods are explored: 2 analytical models (Mori-Tanaka and Mori-Tanaka-Lielens), 1 semi-empirical (Chamis) and 1 finite-element (FE) homogenization (randomly distributed fibres in a Representative Volume Element). Next, the identified fibre properties are used to predict the elastic parameters of UD plies with multiple fibre volume fractions. These are then used to model the fibre bundles (yarns) in a meso-scale FE model of a plain woven carbon/epoxy material. Finally, the predicted elastic response of the woven carbon/epoxy is compared to the experimentally obtained elastic stiffness tensor. The predicted and measured properties are in good agreement. Some discrepancy exists between the ultrasonically measured value of the Poisson's ratio and the predicted value. Nonetheless, it is shown that virtual identification and prediction of mechanical properties for woven plies is feasible.

Keywords: Multiscale modeling, Constituent Property Identification, Textile composites, UD Composites, Ultrasonic Testing

1. Introduction

Multiscale modelling for fibre reinforced composites promises more accurate prediction of the stiffness and the occurrence of several subcritical damage mechanisms up until final failure of the composite materials. In practice, this is done by modelling the small scale constituents and their interactions as individual entities. For Fibre Reinforced Plastics (FRP), the existing approaches can be categorized according to the length scale on which these entities are

*Corresponding author
Email address: ruben.sevenois@ugent.be (R.D.B. Sevenois)
URL: composites.ugent.be (R.D.B. Sevenois)

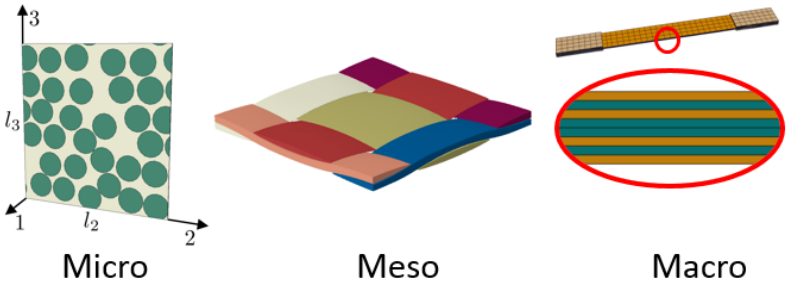

Figure 1: Length scales in multiscale modelling of FRPs

distinguished, figure 1. The micro-scale, where fibres, matrix and fibre-matrix interface are modelled, is used for the modelling of microcracking in Uni-Directional (UD) composite plies [1, 2, 3, 4, 5, 6]. The meso-scale, where fibre bundles and matrix are distinguished, is an intermediate scale for woven [7, 8, 9, 10] or braided [11, 12, 13] composites. Regardless of whether these models are based on an analytical or Finite Element (FE) framework, the separate treatment of the constituents requires their individual mechanical properties as input. However, the datasheets of manufacturers typically only contain the stiffness and strength of the fibre in the fibre direction [14] and the properties of the cured composite layer [15] in the plane of the ply. Typically, no mention is made of the properties of pure matrix or transverse properties of the fibres.

Indeed, the mechanical properties of the pure matrix can be obtained using standard testing methods on pure matrix samples. The properties of the fibres in the shear and transverse direction with respect to the main fibre axis are however not easily determined. There exist experimental methods to determine them. Examples are Dynamic Mechanical Analysis (DMA) or microscopy in combination with single fibre testing [16, 17, 18, 19, 20]. These methods, however, require specialized equipment which is not present in every laboratory and are often combined with specific (analytic) models to identify the searched property.

Researchers often bridge the knowledge gap of unknown mechanical properties by assuming that values for comparable materials from other literature sources apply to their material. Popular reference works are [4, 21]. Examples of where these are referenced include but are not limited to [2, 7, 22, 23, 24, 25]. Another approach is to reverse engineer the constituent properties from macro-scale experimental results. This was extensively used in the recent composite failure prediction benchmark organized by the Air Force Research Laboratory [26, 27] where several participants calibrated the constituent properties on the available experimental data [28, 29].

Note that, although the reverse engineering approach is promising, it can only be used to estimate the properties of the constituent fibres and matrix in micro-scale models. For fibre bundles, the variability in shape, placement and fibre volume fraction [7] provides significantly more variables. Unless detailed information on the placement of the fibre bundles is available, reverse engineering the fibre bundle properties directly using a meso-scale model from the constituent material cannot be done. The situation is different when the properties of the fibre bundles could be determined when it is assumed that fibre bundles can be discretized as UD plies. When the fibre and matrix properties are known, one can analyze multiple micromodels at several fibre volume fractions. In that case the homogenized UD ply properties can be used as input for the fibre bundles leading to the prediction of woven ply macro properties.

Since the properties are carried and identified along multiple scales, a comparison of the latter to the experimental evidence provides a validation of the multiscale modelling approach. When successful, the procedure not only provides confidence in reverse engineering of fibre and matrix properties but also provides a basis for virtual optimization of the woven fibre architecture.

In this work, the authors propose a complete multiscale procedure for the prediction of woven ply elastic properties starting from reverse engineered fibre and matrix properties. The idealized procedure for this using 3D ultrasonic insonification is shown in figure 2. First the knowledge gap in experimental ply properties is bridged by identifying the 3D elastic stiffness tensor for a UD laminate using contact ultrasonics in both through transmission and pulse-echo mode [30]. The 3D elastic properties of the matrix and fibres are reverse engineered followed by a prediction of the homogenized properties of a UD ply at a range of fibre volume fractions. These predictions are then used as input for the fibre bundles in a meso-scale plain woven model. As depicted in the ideal procedure, figure 2, it is attempted to compare the outcome of the meso-scale model to the 3D elastic stiffness tensor from the woven laminate. Unfortunately, determination of the tensor via ultrasonic insonification was not possible due to large attenuation in the signal. As alternative, the predictions by the meso-scale model are compared to the measured experimental properties from standard tensile testing of the woven laminate.

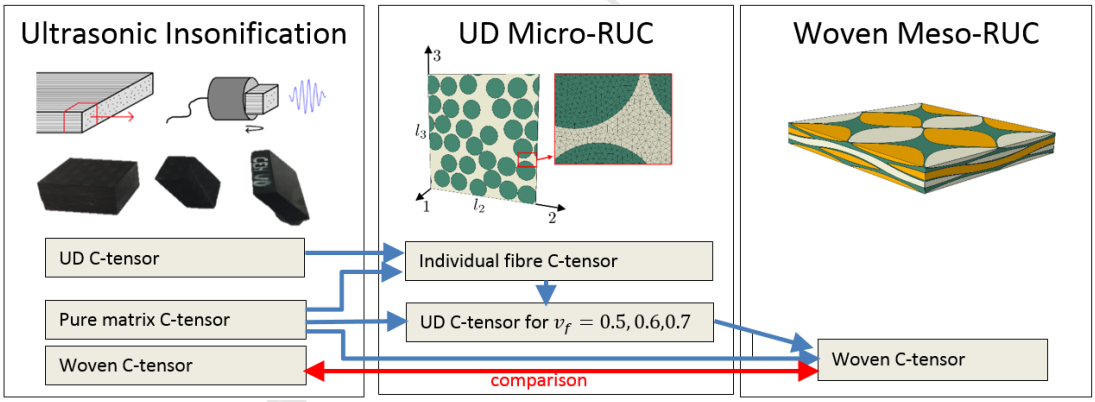

Figure 2: Ideal procedure for the identification of fibre properties and the prediction of the homogenized C-tensor for a woven composite using ultrasonic insonification

In the next sections, first the experimental characterization using contact ultrasonics is given. This is followed by the identification of the fibre and matrix properties from the experimental elastic tensor in Section 3 and the forward prediction of the woven material properties in Section 4. Section 5 contains the conclusions.

2. Experimental Characterization

Ultrasonic testing relies on the fact that the speed of propagation of ultrasound waves through a solid depends on the mechanical properties of that medium. Provided that the time-of-flight (TOF) can be recorded with sufficient accuracy, ultrasonic wave speeds can be determined along different symmetry planes, from which the elastic properties of a laminate can be derived [31, 32]. To study the behaviour of a fibre in UD and woven configuration, it is important that the same fibres and matrix are used in both variants. Therefore the material selected is Pyrofil

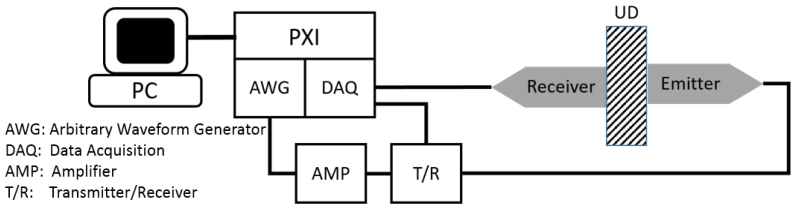

Figure 3: Schematic overview of the contact ultrasonic setup

TR/360 Carbon/Epoxy by Mitsubishi Chemical Corporation because both a UD variant (TR 360E250S) and a plain weave (TR3110 360GMP) exist for this material.

The contact ultrasonic pulse-echo and through-transmission methods were used to measure the phase velocity of both longitudinal and transversal polarized bulk waves along different symmetry planes of small cubes cut from the materials. A schematic overview of the experimental setup can be found in figure 3.

Broadband transducers (longitudinal: Olympus V110-RM and GE H5K, shear: Olympus V156-RM) were put on opposite sides of a small piece of composite material with coupling gel (longitudinal: glycerin based contact gel (GymnaUniphy, Bilzen, Belgium), shear: high viscosity shear gel (Sonotech, Bellingham, WA)), such that the faces of the transducers were between 3 mm and 15 mm apart. For the waveform generation a NI PXI-5412 card (National Instruments Corporation) and an AR 150A100B power amplifier (Amplifier Research) were used, while data acquisition was handled by a NI-PXI-5122 card (National Instruments Corporation).

A 2.5 MHz single-cycle sine burst with Hamming window was given as an input signal. Signals were recorded with a sampling frequency of 100 MSamples/s. Time-domain averaging was used in order to increase the Signal-to-Noise-Ratio (SNR) of the recorded echoes. Multiple echoes in the transmission signal were cross-correlated. The first echoes of the respectively transmission and reflection signals were used to retrieve the TOF of the bulk waves in the material and subsequently the wave velocities could be calculated. At certain symmetry planes the Christoffel equation for orthotropic media yields a set of closed formulas from which the elastic parameters can be determined using phase velocity of ultrasonic bulk waves [32].

Given ρ the density of the material, $v_{i,i}$ the velocity of a longitudinal wave traveling in the x_i direction, $v_{i,j}$ with $i \neq j$ a shear wave traveling in the x_i direction and with a particle displacement in the x_j direction and $v_{ij,ij}$ a quasi-longitudinal or quasi-shear wave traveling in the $x_i x_j$ plane, the relation between the elements of the C-tensor

and the ultrasonic wave velocities can be written down as [32] (Voigt notation):

$$C_{11} = \rho v_{1,1}^2 \tag{1}$$

$$C_{22} = \rho v_{2,2}^2 \tag{2}$$

$$C_{33} = \rho v_{3,3}^2 \tag{3}$$

$$C_{44} = \rho v_{2,3}^2 \tag{4}$$

$$C_{55} = \rho v_{1,3}^2 \tag{5}$$

$$C_{66} = \rho v_{1,2}^2 \tag{6}$$

$$C_{12} = \sqrt{(C_{11} + C_{66} - 2\rho v_{12,12}^2)(C_{22} + C_{66} - 2\rho v_{12,12}^2)} - C_{66} \tag{7}$$

$$C_{13} = \sqrt{(C_{11} + C_{55} - 2\rho v_{13,13}^2)(C_{33} + C_{55} - 2\rho v_{13,13}^2)} - C_{55} \tag{8}$$

$$C_{23} = \sqrt{(C_{22} + C_{44} - 2\rho v_{23,23}^2)(C_{33} + C_{44} - 2\rho v_{23,23}^2)} - C_{44} \tag{9}$$

With these formulas the stiffness tensor values are calculated. The results of the ultrasonic characterization of the UD laminates are shown in table 1 together with the in-plane mechanical properties obtained from standard tensile testing. One can observe that the results obtained from standard tensile testing are lower than measured with ultrasound. This especially for the entries whose behaviour is dominated by the matrix material such as E_{22} and G_{12}. This difference is expected since the ultrasound inhibits high strain rates in the material resulting in stiffer mechanical properties due strain rate dependent behaviour of the polymer matrix.

Table 1: Stiffness tensor coefficients and corresponding engineering properties for the UD laminate determined by ultrasonic and quasi-static measurements

	Ultrasonic			Ultrasonic		Exp. static [33, 34, 35]
Stiffness tensor	Value	Standard Deviation	Engineering Property	Value	Standard Deviation	Value
C_{11} [GPa]	136.50	(1.04)	E_1 [GPa]	135.37	(1.08)	129.95
C_{22} [GPa]	12.54	(0.60)	E_2 [GPa]	11.36	(0.24)	8.34
C_{33} [GPa]	12.73	(0.15)	E_3 [GPa]	11.53	(0.29)	-
C_{44} [GPa]	3.26	(0.05)	ν_{12} [-]	0.20	(0.06)	0.34
C_{55} [GPa]	5.40	(0.28)	ν_{13} [-]	0.17	(0.06)	-
C_{66} [GPa]	5.40	(0.35)	ν_{23} [-]	0.37	(0.02)	-
C_{12} [GPa]	3.04	(0.60)	G_{12} [GPa]	5.40	(0.35)	4.68
C_{13} [GPa]	3.08	(0.60)	G_{13} [GPa]	5.40	(0.28)	-
C_{23} [GPa]	4.73	(0.27)	G_{23} [GPa]	3.23	(0.05)	-

A UD laminate is often assumed to behave transversely isotropic. The relationships between the entries of the

stiffness tensor for transverse isotropic properties are shown below:

$$C_{22} = C_{33} \tag{10}$$

$$C_{12} = C_{13} \tag{11}$$

$$C_{55} = C_{66} \tag{12}$$

$$C_{23} = C_{22} - 2C_{44} \tag{13}$$

Testing the relationships between the experimentally determined values it is observed that, considering the given standard error, the relationship (13) between C_{23} and C_{22}, C_{44} does not seem to hold. Additionally, when computing the engineering properties for the laminate, it is noted that the in-plane Poisson's ratio, computed as $\nu_{12} = 0.176$, is small. From standard tensile testing according to ASTM D3039 [36] a Poisson's ratio of $\nu_{12} = 0.335$ (Table 2) was reported for this laminate. The difference is large, even considering rate dependency effects due to the high strain rate exerted on the material by the ultrasonic waves. A possible explanation for these two observations can be found in the experimental C-tensor identification procedure. This together with the large differences in Young's moduli for the different directions of the laminate makes the identification procedure for the C-tensor values ill-conditioned for the entries C_{12}, C_{13} and C_{23}. Small variations in the measurements can therefore result in a large variation in the identified values.

Because the selected material models result in transversely isotropic behaviour, the values of the stiffness tensor are corrected and idealized. The small variation between longitudinal and shear coefficients, which should be equal, are recalculated as the mean value of the experimental ones, $C_{22} = C_{33} = 0.5(C^0_{22} + C^0_{33})$, $C_{55} = C_{66} = 0.5(C^0_{55} + C^0_{66})$, and $C_{12} = C_{13} = 0.5(C^0_{12} + C^0_{13})$. The value for C_{23} is recalculated according to the equation (13). This is the unadapted property set. Next to these initial corrections a third set of C-tensor values is produced with the adaptation $\nu_{12} = 0.335$. The resulting values are shown in table 2.

Table 2: Stiffness tensor coefficients for the UD laminates

Stiffness tensor	Original	Transv. Iso. Unadapted	Transv. Iso. $\nu_{12} = 0.335$ Adapted
C_{11} [GPa]	136.50	136.50	139.44
C_{22} [GPa]	12.54	12.64	12.83
C_{33} [GPa]	12.73	12.64	12.83
C_{44} [GPa]	3.26	3.26	3.26
C_{55} [GPa]	5.40	5.40	5.40
C_{66} [GPa]	5.40	5.40	5.40
C_{12} [GPa]	3.04	3.06	5.95
C_{13} [GPa]	3.08	3.06	5.95
C_{23} [GPa]	4.73	6.13	6.32

The same ultrasonic identification of the 3D elastic tensor is done for the pure matrix material and for the woven material. The resulting stiffness properties of the pure matrix are shown in table 3. For comparison, the properties measured using standard quasi-static methods are shown as well. As can be seen in the table, there is a large difference between the measurements by quasi-static and ultrasound. This is also attributed to strain rate dependent behaviour.

Unfortunately, the ultrasonic signals for the woven material show a large attenuation. This is probably caused by the undulation of the fibre bundles within a ply. Consequently, the elastic properties cannot be obtained with sufficient confidence using this method. Therefore, the idealized procedure proposed in figure 2 cannot be completed at this time. To provide a comparison between predicted and experimentally obtained values of the woven material, the in-plane properties of the woven laminate are determined using standard tensile tests according to ASTM D3039 [36] and ASTM D3518 [37]. Further discussion on this topic is given in Section 4.

Table 3: Stiffness properties of pure epoxy matrix from ultrasound and quasi-static

	Ultrasound	Exp. static [38, 39]
E [GPa]	3.70	3.00^b
ν [−]	0.40	0.42^b
G [GPa]	1.32^a	0.97^c

[a] Isotropic assumption $G = E/(2(1+\nu))$ [b] Static tensile test [c] ASTM D5379 Iosipescu shear test

3. Identification of Transverse Isotropic Fibre Properties

The fibre properties cannot be determined directly from the experimental data. Therefore, they have been identified through reverse engineering using a homogenization method [40]. A micro-mechanical model based on the material properties of its constituents and its micro-structure is needed to determine the homogenized properties of a UD laminate. In a general micro-mechanical model the homogenized stiffness tensor of the UD laminate $\widetilde{C}^{\mathrm{UD}}$ can be written as a function of the stiffness tensors of the matrix C^m and fibres C^f as follows:

$$\widetilde{C}^{\mathrm{UD}} = h(C^f, C^m) \tag{14}$$

where the function h takes into account the micro-structure of the UD laminate. This relationship cannot be inverted analytically, and the fibre properties must be obtained using an iterative identification until the homogenized stiffness tensor $\widetilde{C}^{\mathrm{UD}}$ matches with the experimental data C^{UD}. The steps to calculate the fibre properties are described in the next sections.

3.1. Micro-structure of the UD laminate

Figure 4 (a) shows a micrograph of the UD laminate. A magnification of the Figure is shown in the enlargment in (c). The distribution of fibres is not uniform showing a random pattern. From this figure the fibre volume fraction is calculated as the ratio between the area occupied by fibres and the total area of a selected region. Note that the size and location of the region can influence the calculated fibre volume fraction due to the existence of a matrix rich region located at the interface of neighboring plies. The local volume fraction changes from 0.49 in the region between plies to 0.68 in the middle of each ply. On average the fibre volume fraction of the laminate is 0.6. The latter has been calculated from several micrographs along the thickness of the laminate.

In order to define the homogenization function of equation (14), four micro-structure models have been chosen. Two analytical models, namely, Mori-Tanaka [41, 42] and Mori-Tanaka-Lielens (interpolation of double inclusion

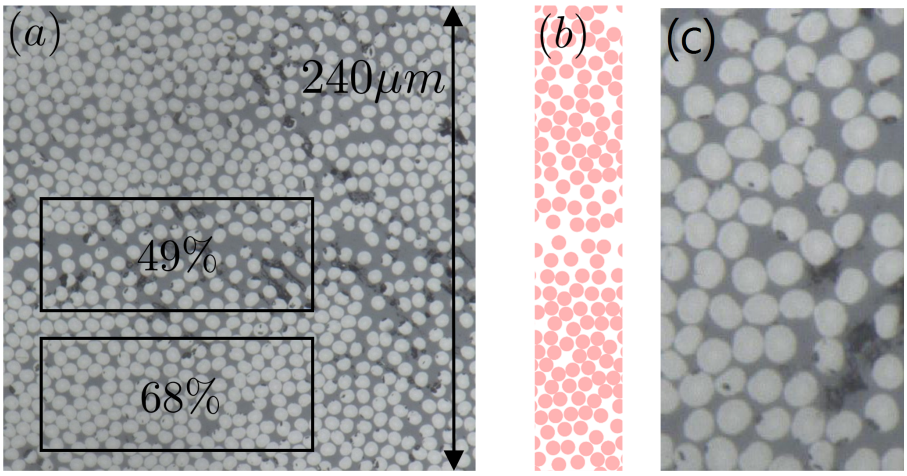

Figure 4: Microscope image of the UD laminate with local volume fractions (a), corresponding fibre distribution model (b) and close-up (c)

formulation) [43]; one semi-empirical model, Chamis [44]; and a finite element model based on a Representative Volume Element (RVE) that mimics the random distribution of fibres, see figure 4 (b).

The analytical and semi-empirical homogenized models used in this study assume that the fibers are infinite cylindrical inclusion oriented in one direction with a uniform distribution in the plane transverse to the fibers. They are formulated in a closed form with the stiffness tensors. Therefore, the homogenized properties of the UD laminate $\widetilde{C}^{\mathrm{UD}}$ are computed directly from the stiffness tensor of the matrix C^m and the guessed stiffness tensor of the fibres C^f. On the other hand, the finite element model retains additional information about the micro-structure, such as the random distribution of fibres and the non-uniformity of the volume fraction. As a disadvantage, there is no closed form of the formulation and an iterative procedure is necessary to obtain a solution. Then, it is needed to perform one FE simulation per iteration which involves higher computational cost.

3.2. Micro-mechanical model based on finite elements

The geometry of the model is given by a periodic RVE which is a cuboid composed of a random distribution of cylindrical fibres parallel to direction 1, see figure 5. The radius of the fibres is known, $r^f = 3.6$ microns, and the volume fraction is fixed, $v_f = 0.6$. Therefore, the dimensions of the transverse section l_2 and l_3 are calculated from the number of fibres n^f, r^f and v_f assuming an initial hexagonal distribution. Because of the imposed periodicity in the direction of the fibres, l_1 is not relevant for the results. To minimize the computational effort, only one layer of elements is used in this direction and l_1 is determined by the element size.

The random distribution of fibres is generated with a simple collision model which keeps the general v_f constant in a prefixed domain [45, 46]. A script in Octave [47] is used to generate different RVEs with a total of 30 fibres. Next to that a RVE with 150 fibres is generated as well, where the non-uniform fibre volume fraction through the ply-thickness is mimicked, see figure 4 (b).

The geometry is discretized using wedge elements with 6 nodes and 2 integration points (C3D6 [48]), see figure 5. It is verified that a global element size of 0.3 μm ensures converged predictions of the homogenized elastic properties

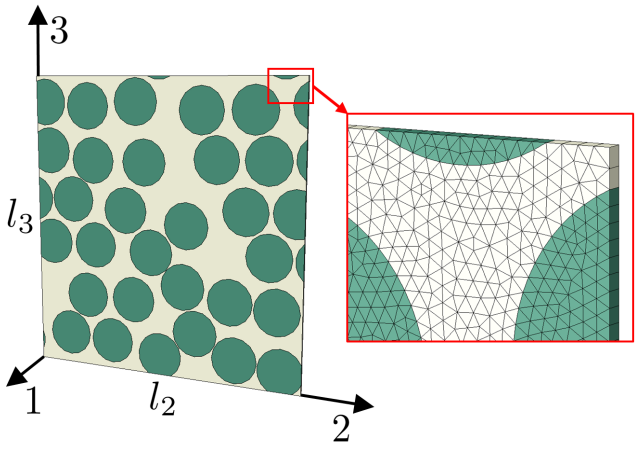

Figure 5: RVE with 30 fibres and mesh detail.

for the RVE. Periodic Boundary Conditions (PBCs) [49] are applied between the three pairs of parallel faces of the geometry. The homogenized elastic properties are obtained by imposing 6 load cases, three longitudinal and three shear strains (ε_{11}, ε_{22}, ε_{33}, ε_{23}, ε_{13}, ε_{12}), as macro-strains via the PBCs. For each load case, the stress field at the integration points is obtained. Weighted volume averaging of the stress field in combination with the imposed macro-strains results in the homogenized stiffness tensor of the UD laminate.

$$\sigma_i = \frac{\sum_{k=1}^{N} \sigma_i^k V^k}{\sum_{k=1}^{N} V^k} \tag{15}$$

$$C_{ji} = \frac{\sigma_i}{\varepsilon_j} \tag{16}$$

where σ_i is the average stress, V^k and σ_i^k are the volume and stress in the k-th node for direction i = 1,...,6 (Voigt notation). ε_j is the j-th strain load ($j = 1, ..., 6$ Voigt).

3.3. Iterative identification method of fibre properties

Since the fibre stiffnes tensor C^f cannot be directly obtained from equation (14) for the selected micro-structure models, an iterative method is used to estimate it. The iterative method is based on the secant method. The analysis is started by assuming two starting values for the fibre stiffness tensor $[C^f]^{0,1}$. The initial guesses are determined using the rule of mixtures and Mori-Tanaka,

$$[C^f]^0 = (C^{\mathrm{UD}} - (1 - v_f)C^m)/v_f \tag{17}$$

$$[C^f]^1 = (C^{\mathrm{UD}}((1 - v_f)I + v_f T^f) - (1 - v_f)C^m)(v_f T^f)^{-1} \tag{18}$$

where the strain concentration tensor $T^f = (I + \xi((C^m)^{-1}C^f - I))$ is computed with the fibre stiffness tensor from the first guess $C^f = [C^f]^0$, I is the identity matrix (6x6), and ξ is the Eshelby tensor for cylindrical inclusions [50, 51].

The guessed fibre tensors and the matrix tensor are used in the homogenized model to obtain the homogenized

stiffness tensor of each iteration i given by:

$$[\tilde{C}^{\mathrm{UD}}]^i = h\left([C^f]^i, C^m\right) \tag{19}$$

Then, the new value for the fibre stiffness tensor is determined using

$$[C^f_{mn}]^{i+1} = [C^f_{mn}]^i - [\Phi_{mn}]^i \frac{[C^f_{mn}]^i - [C^f_{mn}]^{i-1}}{[\Phi_{mn}]^i - [\Phi_{mn}]^{i-1}} \tag{20}$$

where $[\Phi]^i$ is the residual stiffness tensor calculated as the difference between the experimental and homogenized stiffness tensor of the UD laminate, $[\Phi]^i = [C^{\mathrm{UD}}]^i - [\widetilde{C}^{\mathrm{UD}}]^i$. It is important to mention that equation (20) is computed per coefficient with $m, n = 1, 2, 3, 4, 5, 6$.

The new value for the fibre stiffness tensor is reintroduced in the homogenization method and the procedure is repeated until the coefficients of $[\Phi]^i$ are below a certain tolerance. To be in agreement with the accuracy of the experimental data, this tolerance must be lower than the last significant figure of the experimental stiffness coefficients. In this work a tolerance of 10^{-6} is used to reach a precision of 4 significant figures.

3.4. Identification of fibre properties

The carbon fibres are commonly assumed to have transversely isotropic properties due to their internal structure and the cylindrical geometry. Therefore, the orthotropic stiffness tensor is simplified using (10)-(13) to a stiffness tensor with only 5 independent coefficients.

Table 4 shows the fibre properties from the iterative identification for the experimental data assuming the transversely isotropic data presented in table 2 and some popular fibre property datasets from literature. The results have been obtained for each micro-structural model: Mori-Tanaka (MT), Mori-Tanaka-Lielens (MTL), Chamis and the FE-RVE model with 30 fibres. To take into account the randomness distribution of fibres in the RVE, the calculated fibre properties are an average of the properties from 3 different configurations. The small dispersion warrants that the RVE with 30 fibre contains sufficient fibres to give representative values.

There was some concern that the existence of non-evenly distributed fibre volume fraction in the ply and at ply interface could influence the elastic properties of the laminate. The RVE of 150 fibres, with the non-uniform fibre volume fraction, however, only shows slight orthotropic behaviour. The longitudinal components C_{22}, C_{33} and the shear components C_{12}, C_{13} differ by 1%. More remarkable differences up to 4% are seen between the shear components C_{55} and C_{66}. There is a difference of 4% between the coefficient C_{23} and the ideal value for transverse isotropic behaviour calculated from equation (13). These deviations from the transverse isotropic behaviour are not sufficiently large to explain the 21% difference between the experimental and the transverse isotropic experimental value for C_{23} mentioned in section 2.

The identified fibre properties from the analytical models, Mori-Tanaka (MT) and Mori-Tanaka-Lielen (MTL), show a range for the stiffness and Poisson's ratio values. Other investigations about the accuracy of these methods show that MT gives homogenized stiffness values higher than the experimental ones while MTL underestimates the homogenized stiffness values [54, 55]. Therefore, the identified fibre properties by MT can be taken as upper bounds

Table 4: Transverse isotropic fibre properties for each different micro-model and reference data from literature.

Micro-structure	Mori-Tanaka	Mori-Tanaka-Lielen	Chamis	FE	AS4 ref.[52]	T300 ref.[53]
E_1^f [GPa]	223.101	222.350	223.366	223.300	235	230
E_2^f [GPa]	20.764	14.776	18.107	18.365	14	8-13.4
E_3^f [GPa]	20.764	14.776	18.107	18.365	14	8-13.4
ν_{12}^f [-]	0.018	0.054	0.006	0.022	0.2	0.256
ν_{13}^f [-]	0.018	0.054	0.006	0.022	0.2	0.256
ν_{23}^f [-]	0.182	0.366	0.599	0.269	0.25	0.3
G_{12}^f [GPa]	> 1000	14.619	51.951	36.898	28	27.3
G_{13}^f [GPa]	> 1000	14.619	51.951	36.898	28	27.3
G_{23}^f [GPa]	8.781	5.407	5.661	7.241	5.5	3.08

for the stiffness and lower bounds for the Poisson's ratio. On the contrary, for the MTL, the identified properties can be taken as lower bounds for stiffness and upper bound for Poisson's ratio. It is noteworthy that MT model reports unrealistically high shear stiffness, G_{12}^f and G_{13}^f, for the ultrasonic input data assuming a volume fraction of 60%. The source of this unrealistic value is the closed form formulation of G_{12} for M-T in [51]. The formulation is shown in Equation 21 from which it can be observed that G_{12} is inversely proportional to G_{12}^f. Because of this, the dependency of G_{12} on G_{12}^f diminishes with increasingly higher values. As a result, G_{12} reaches a plateau at high values of G_{12}^f. For this dataset, and with the volume fraction of 60%, this plateau is lower than the experimentally observed value which explains the unrealisticly high value for G_{12}^f.

$$G_{12} = G_{13} = \frac{E_m}{2(1-f)(1+\nu_m)} \left(1 + f - 4f \left\{ 1 + f + 2(1-f)\frac{G_{12}^f}{E_m}(1+\nu_m) \right\}^{-} 1 \right) \tag{21}$$

Table 4 also shows the identified fibre properties obtained with Chamis and FE-RVE. In the past, Chamis has been used successfully to identify fibre properties for different composites from carbon fibre and glass fibre [56]. The stiffness values calculated with Chamis' model for our experimental data are between the bounds given by MT and MTL. However, the Poisson's ratios are out of these bounds. For the FE model, the identified carbon fibre properties are between the bounds of MT and MTL and close to the stiffness values identified with Chamis.

For all the micro-structural models, the Poisson's ratio ν_{12}^f of the fibres is small compared with the usually reported value of around 0.2 [4, 52, 53], see table 4. This is a direct effect of the small experimentally obtained value of the UD laminate $\nu_{12} = 0.176$. Because the ill-conditioned values for C_{12} and C_{13}, a second identification of fibre properties has been done assuming $\nu_{12} = 0.335$ for the UD laminate, see table 2. The fibre properties of the first identification (Set 1) and the second identification (Set 2) are compared in table 5. In the second identification $\nu_{12}^f = 0.26$, this value is close to the reported ones. The other properties have negligible differences between both sets. The values of the standard deviation calculated from the 3 configurations of RVEs with 30 fibres are also shown in table 5 for each set of properties. Except the standard deviation of ν_{12}^f and ν_{13}^f for the Set 1, all the rest are below 5%.

3.5. Prediction of properties of UD laminate

With the material properties of each constituent, fibre and matrix, the properties of UD laminates with different volume fractions v_f are calculated by means of finite elements. The UD laminate properties for v_f between 50% and

Table 5: Transverse isotropic fibre properties using FE-RVE for UD laminates with different ν_{12}

Micro-structure	Set 1 ($\nu_{12} = 0.176$)		Set 2 ($\nu_{12} = 0.335$)	
E_1^f [GPa]	223.300	(0.017)	223.987	(0.052)
E_2^f [GPa]	18.365	(0.212)	18.534	(0.217)
E_3^f [GPa]	18.365	(0.212)	18.534	(0.217)
ν_{12}^f [-]	0.022	(0.002)	0.258	(0.004)
ν_{13}^f [-]	0.022	(0.002)	0.258	(0.004)
ν_{23}^f [-]	0.269	(0.022)	0.282	(0.022)
G_{12}^f [GPa]	36.898	(2.111)	36.898	(2.111)
G_{13}^f [GPa]	36.898	(2.111)	36.898	(2.111)
G_{23}^f [GPa]	7.241	(0.212)	7.232	(0.210)

90% are calculated using the 30 fibre RVE for the two sets of carbon fibre properties, table 5. The results are shown in table 6 and 7, respectively. The same identification is done using the identified properties from MTL for which the results are shown in table 8.

Table 6: Predicted homogenized properties for a UD yarn for $v_f = 0.50 - 0.90$ with Set 1 of fibre properties.

Volume fraction v_f	0.50	0.55	0.60	0.65	0.70	0.75	0.80	0.85	0.90
E_1 [GPa]	113.55	124.53	135.50	146.46	157.41	168.36	179.31	190.25	201.21
E_2 [GPa]	8.27	9.02	9.65	10.48	11.14	12.10	13.16	14.23	15.58
E_3 [GPa]	8.27	9.02	9.65	10.48	11.14	12.10	13.16	14.23	15.58
ν_{12} [-]	0.20	0.183	0.164	0.15	0.13	0.109	0.09	0.07	0.06
ν_{13} [-]	0.20	0.183	0.164	0.15	0.13	0.109	0.09	0.07	0.06
ν_{23}[-]	0.52	0.496	0.480	0.46	0.44	0.416	0.39	0.36	0.33
G_{12} [GPa]	3.85	4.52	5.31	6.384	7.45	8.80	11.18	13.97	21.37
G_{13} [GPa]	3.85	4.52	5.31	6.384	7.45	8.80	11.18	13.97	21.37
G_{23} [GPa]	2.72	2.93	3.23	3.538	3.96	4.30	4.72	5.23	5.86

Table 7: Predicted homogenized properties for a UD yarn for $v_f = 0.50 - 0.90$ with Set 2 of fibre properties.

Volume fraction v_f	0.5	0.55	0.6	0.65	0.7	0.75	0.8	0.85	0.9
E_1 [GPa]	113.78	124.74	135.74	146.74	157.74	168.74	179.73	190.73	201.74
E_2 [GPa]	8.26	9.02	9.66	10.50	11.16	12.13	13.21	14.30	15.68
E_3 [GPa]	8.26	9.02	9.66	10.50	11.16	12.13	13.21	14.30	15.68
ν_{12}[-]	0.33	0.32	0.31	0.30	0.30	0.29	0.28	0.28	0.27
ν_{13}[-]	0.33	0.32	0.31	0.30	0.30	0.29	0.28	0.28	0.27
ν_{23} [-]	0.52	0.50	0.48	0.46	0.45	0.42	0.39	0.37	0.34
G_{12} [GPa]	3.85	4.52	5.31	6.38	7.45	8.79	11.18	13.97	21.37
G_{13} [GPa]	3.85	4.52	5.31	6.38	7.45	8.79	11.18	13.97	21.37
G_{23} [GPa]	2.72	2.93	3.23	3.54	3.96	4.30	4.72	5.23	5.86

Comparing the three tables, it can easily be seen that the differences in single fibre properties are projected on the predicted UD laminate properties. For example, fibre property Set 2 has the highest Poisson's ratio and consequently the predicted properties using this set for the UD laminate have the highest Poisson's ratio. In the next section it is shown whether the same observation can be made when the UD laminate properties are used to predict the properties of the woven material.

Table 8: Predicted homogenized properties for a UD yarn for $v_f = 0.50 - 0.90$ with the fibre properties of MTL.

Volume fraction v_f	0.5	0.55	0.6	0.65	0.7	0.75	0.8	0.85	0.9
E_1 [GPa]	113.55	124.52	135.49	146.46	157.41	168.37	179.32	190.27	201.23
E_2 [GPa]	7.62	8.18	8.67	9.29	9.78	10.48	11.24	11.99	12.90
E_3 [GPa]	7.62	8.18	8.67	9.29	9.78	10.48	11.24	11.99	12.90
ν_{12}[-]	0.22	0.20	0.19	0.17	0.15	0.14	0.12	0.10	0.09
ν_{13}[-]	0.22	0.20	0.19	0.17	0.15	0.14	0.12	0.10	0.09
ν_{23}[-]	0.55	0.53	0.51	0.50	0.49	0.47	0.45	0.43	0.41
G_{12} [GPa]	3.34	3.78	4.27	4.89	5.52	6.25	7.32	8.53	10.68
G_{13} [GPa]	3.34	3.78	4.27	4.89	5.52	6.25	7.32	8.53	10.68
G_{23} [GPa]	2.47	2.63	2.85	3.06	3.35	3.59	3.87	4.20	4.58

4. Prediction of Woven Ply Elastic Properties

The prediction of the mechanical properties of a woven ply is carried out using a Representative Unit Cell (RUC) at the meso-scale where two ingredients are required: (i) knowledge about the geometrical placement of the yarns in the laminate structure to construct and mesh the RUC and (ii) knowledge about the mechanical properties of the constituents (yarns and matrix) that will be assigned to each geometrical region.

Knowledge about the geometrical arrangement of the fibre bundles in the laminate has been obtained by the authors in a previous work [7]. Detailed in-situ measurements of the fibre bundle shape throughout the structure were obtained from micro Computed Tomographic X-ray (microCT) scans of the material. The shape of the yarns was analyzed from which it was concluded that the general method for constructing RUCs (using simple shape functions) is insufficient to correctly represent them. Specifically, the inability to achieve a realistic representation of ply nesting and the variation in shape of the yarn along its path are limiting factors. To resolve this, a new method for the construction of a meso-RUC was proposed. The Measurement Enhanced Shape Identification (MESI) method uses a general and periodic form of the superelliptic function to provide smoothly varying closed yarn regions. The transverse shape of the yarn is defined with a general form of the superelliptic function:

$$\left|\frac{x}{2w_{\text{yarn}}(y)}\right|^{c_{\text{top}}(y)} + \left|\frac{z}{2h_{\text{yarn}}(y)}\right|^{c_{\text{tip}}(y)} = 1 \tag{22}$$

where $2w_{\text{yarn}}$ and $2h_{\text{yarn}}$ are the lengths of the major and minor axis, respectively yarn width and height. c_{tip} and c_{top} are two fitting parameters that control the shape curvature. y is the yarn lengthwise direction. The variation of the heartline is defined with a periodic form of the generalized superellipse:

$$f(y) = b\frac{\left|\text{Cos}\left(\pi\frac{1}{2a}y\right)\right|}{\text{Cos}\left(\pi\frac{1}{2a}y\right)}\left[1 - \left|\frac{y - a\text{Round}\left[\frac{y}{a}, 2\right]}{a}\right|^{c_1}\right]^{(1/c_2)} + e \tag{23}$$

where Round$[x, 2]$ is a rounding of x to the nearest multiple of 2, a is one fourth of the period of the signal, b is the amplitude and e is the mean through thickness height. The curvature can again be tuned using c_1 and c_2. Note that the dependency of the shape parameters in the y-direction allows to obtain the aforementioned smooth variable cross section along the yarn heartline.

The effect of the curvature parameters and possible yarn shapes and heartline paths are illustrated in figure 6

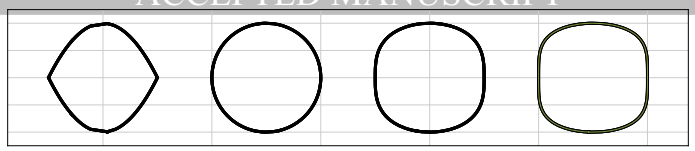

Figure 6: Superelliptic shapes with $c_{\text{top}} = 2$ and $c_{\text{tip}} = 1, 2, 3, 4$ [7]

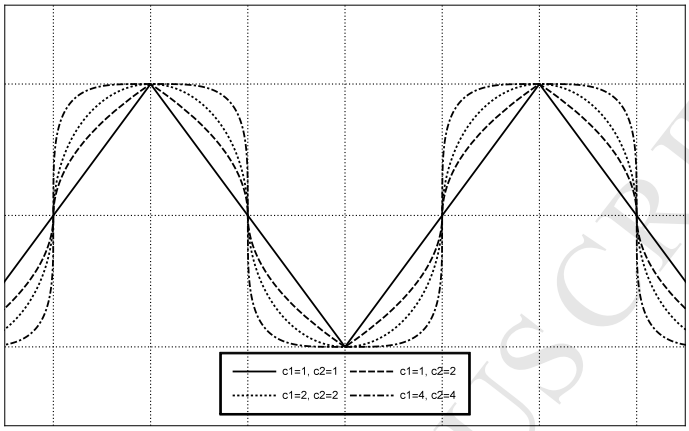

Figure 7: Influence of c_1 and c_2 in Equation 23 [7]

and 7. Detailed information on the identification of the shape parameters for this material can be found in [7]. The resulting configuration is a 2-ply RUC shown in figure 8, where the plies are nested out-of-phase to achieve a correct yarn-matrix volume fraction.

A consequence of the variable cross section is that the fibre volume fraction (v_f) of the yarns varies accordingly. This is shown for the warp yarns in steps of 5% v_f in figure 9. Now the value of the multiscale method for material property identification becomes clear. Instead of having to perform multiple cumbersome experiments to determine the properties of the UD material at several fibre volume fractions (table 6), the predictions of the FE model with 30 fibres RVE can readily be used as input for the respective yarn regions. Determining this experimentally is laborious because it is difficult to control the volume fraction during production.

The meso-RUC is meshed with 43,520 C3D20 hexahedrals in the yarns and 532,875 C3D10 tetrahedrals in the matrix resulting in a total of 1,235,692 nodes. The average element edge length is 56.29μm. A mesh convergence

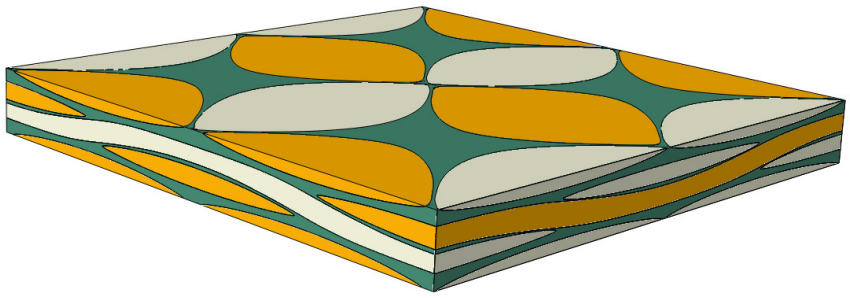

Figure 8: Nested MESI-RUC [7]

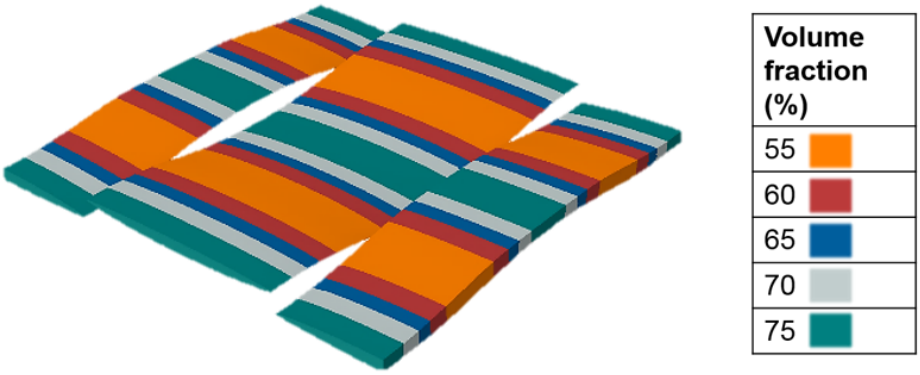

Figure 9: Variation of the fibre volume fraction in the warp yarns

study confirmed that there is convergence of: (i) the homogenized elastic properties, and (ii) the internal yarn and matrix stress fields. Since hexahedrals and tetrahedrals are incompatible elements, yarns and matrix are connected using a surface tie formulation. The PBC and homogenization procedure is the same as used for the FE model with 30 fibres RVE.

The predicted ply properties from the meso-RUC are given in table 9 together with a comparison with the measured properties from the woven material. Between the three homogenization methods and the experimental values, there is small variation in the Young's moduli and the shear moduli G_{13} and G_{23}. Larger differences are seen for the shear modulus G_{12} which is predicted to be 50% higher than the experimentally observed one in both MESI homogenizations.

Indeed, the predicted shear modulus for MESI-MTL is closer to the experiment. This is due to the lower fibre shear modulus predicted by MTL as can be seen in Table 4. Note, however, that although the difference between the fibre shear modulus of MTL and FE-RVE is more than 50%, the homogenized ply shear modulus only dropped by 20%. This illustrates that the fibre modulus only has a limited influence on the shear stiffness. The stiffness of the matrix thus plays a more significant role. Recall that the properties of the matrix were measured using contact ultrasound. Although the ultrasound produces a low strain amplitude in the material, the high frequency causes the material to be strained at higher strain rates than in quasi-static testing. It is known that polymers exhibit viscoelastic behaviour. The stiffness of the material increases with increasing strain rate. Therefore, the elastic properties of the matrix and UD material, obtained from contact ultrasound, are representative for a higher strain rate. Consequently, the predictions by the MESI-RUC in table 9 are valid for high strain rate tests on the woven material. The experimental work on the woven material, however, is obtained using standard tensile testing at a low strain rate. Due to the fact that there are no fibres in the shear direction this comparison suggests that strain rate dependence of the matrix might have a dominating role.

The difference in the assumed Poisson's ratio of the UD material does not seem to have a significant influence. A difference is visible in the prediction of the woven ply Poisson's ratio ν_{12}. The *adapted* version for the woven laminate Poisson's ratio is 40% higher compared with the *unadapted* one. This is a lot less than the initial difference of 90% ($\nu_{12} = 0.176$ vs $\nu_{12} = 0.335$) between the ratios for the UD laminate. Clearly the transverse fibres in the woven material

Table 9: Comparison experimental properties and meso-RUC properties

	Exp. static [57, 58]	MESI	MESI-$\nu_{12} = 0.335$	MESI-MTL
E_1 [GPa]	58.1	60.0	60.3	59.3
E_2 [GPa]	56.7	59.3	59.6	58.6
E_3 [GPa]	-	10.8	10.6	10.2
ν_{12}[-]	0.04	0.05	0.07	0.06
ν_{13}[-]	-	0.41	0.49	0.44
ν_{23}[-]	-	0.41	0.50	0.47
G_{12} [GPa]	3.6	5.1	5.1	4.0
G_{13} [GPa]	-	3.3	3.3	2.9
G_{23} [GPa]	-	3.3	3.3	3.0

restrict the Poisson's contraction reducing the contribution of the yarns' individual Poisson's ratio to the woven ply Poisson's ratio. Yet it is noted that the woven ply Poisson's ratio with $\nu_{12} = 0.176$ is closest to the experimentally observed value.

5. Conclusion

In this work a multiscale method to identify the 3D transverse isotropic elastic properties of carbon fibres from ultrasound measurements of a UD material is presented. The individual fibre and matrix properties are subsequently used to predict the elastic stiffness tensor for woven material from the same fibres and matrix. Considering experimental scatter the meso-RUC is able to predict the properties of the woven ply quite adequately using the homogenized yarn properties from an analytical method and a micro-RVE. The disagreement with the in-plane shear stiffness G_{12} needs to be investigated further.

An important aspect for the identification of fibre properties is the ability to obtain the 3D mechanical properties of the UD laminate. In this work this was done using the ultrasonic testing of small cubes of the UD, woven and matrix material. Also, a number of topics for further investigation are identified. Work needs to be done to resolve the ill-conditioned identification problem. As mentioned in Section 2 the uncertainty in the determination of the Poisson's coefficients C_{12}, C_{13} and C_{23} caused the authors to consider manually *adapting* the ultrasonically measured UD ply Poisson's ratio $\nu_{12} = 0.176$ to the static tensile experimentally measured value of $\nu_{12} = 0.335$. Finally, *adapting* this values does not seem necessary as Poisson's ratio of the woven material is only limitedly influenced, section 4.

Other work needs to be done on the identification of woven ply properties using ultrasonics. This was attempted but aborted due to the large attenuation in transmitted ultrasonic waves. To allow ultrasonic determination of the 3D mechanical properties of the woven material, the cause of the large attenuation needs to be identified. At the moment it is thought that the undulation of the yarns in combination with a plain woven ply cell with approximately the size of the ultrasonic transducers play a role. This will be investigated in future research.

Identification of the fibre properties from the measured UD laminate properties was done with 2 analytical, 1 semi-analytical and 1 FE model based on a RVE. It is shown that, depending on the chosen method, the identified properties can vary considerably. Unfortunately, there are no direct experimental measurements of the full set of elastic coefficients of individual fibres. This prevents to assess which model is the most accurate. The MT and MTL models were identified as the models providing the boundaries within which the fibre properties could lie. It is shown

here that there is negligible difference between the use of MTL or the FE model with a RVE for the identification of fibre properties. Both methods produce equally good predictions.

Although some work remains, two conclusions are drawn from this research: (i) Backward identification of fibre properties from 3D mechanical properties of UD laminates results in acceptable values and (ii) Multiscale prediction of woven properties from fibre and matrix properties leads to good predictions of the ply mechanical properties.

6. Acknowledgement

The work leading to this publication has been funded by the SBO project M3Strength (Grant no. 130546), which fits in the Macro- ModelMat (M3) research program funded by SIM (Strategic Initiative Materials in Flanders) and VLAIO (Flanders Innovation & Entrepreneurship Agency).

References

[1] C. T. Key, S. C. Schumacher, A. C. Hansen, Progressive failure modeling of woven fabric composite materials using multicontinuum theory, Composites Part B: Engineering 38 (2) (2007) 247–257. doi:10.1016/j.compositesb.2006.03.006.
URL http://linkinghub.elsevier.com/retrieve/pii/S1359836806000552

[2] R. D. B. Sevenois, D. Garoz, F. A. Gilabert, S. W. F. Spronk, W. Van Paepegem, Microscale based prediction of matrix crack initiation in UD composite plies subjected to multiaxial fatigue for all stress ratios and load levels, Composites Science and Technology 142 (2017) 124–138. doi:10.1016/j.compscitech.2017.02.004.

[3] M. K. Ballard, J. D. Whitcomb, Effective use of cohesive zone-based models for the prediction of progressive damage at the fiber/matrix scale, Journal of Composite Materials 51 (5) (2017) 649–669. doi:10.1177/0021998316651127.
URL http://journals.sagepub.com/doi/10.1177/0021998316651127

[4] A. Arteiro, G. Catalanotti, A. Melro, P. Linde, P. Camanho, Micro-mechanical analysis of the in situ effect in polymer composite laminates, Composite Structures 116 (2014) 827–840. doi:10.1016/j.compstruct.2014.06.014.
URL http://linkinghub.elsevier.com/retrieve/pii/S0263822314002839

[5] I. Doghri, A. Ouaar, Homogenization of two-phase elasto-plastic composite materials and structures, International Journal of Solids and Structures 40 (7) (2003) 1681–1712. doi:10.1016/S0020-7683(03)00013-1.
URL http://linkinghub.elsevier.com/retrieve/pii/S0020768303000131

[6] I. Doghri, L. Tinel, Micromechanical modeling and computation of elasto-plastic materials reinforced with distributed-orientation fibers, International Journal of Plasticity 21 (10) (2005) 1919–1940. doi:10.1016/j.ijplas.2004.09.003.
URL http://linkinghub.elsevier.com/retrieve/pii/S0749641904001706

[7] R. D. B. Sevenois, D. Garoz, F. A. Gilabert, S. W. F. Spronk, S. Fonteyn, M. Heyndrickx, L. Pyl, D. V. Hemelrijck, J. Degrieck, W. V. Paepegem, Avoiding interpenetrations and the importance of nesting in analytic geometry construction for Representative Unit Cells of woven composite laminates, Composites Science and Technology 136 (2016) 119–132. doi:10.1016/j.compscitech.2016.10.010.
URL http://linkinghub.elsevier.com/retrieve/pii/S0266353816304560

[8] A. Doitrand, C. Fagiano, F. X. Irisarri, M. Hirsekorn, Comparison between voxel and consistent meso-scale models of woven composites, Composites Part A: Applied Science and Manufacturing 73 (2015) 143–154. doi:10.1016/j.compositesa.2015.02.022.
URL http://dx.doi.org/10.1016/j.compositesa.2015.02.022

[9] M. Hirsekorn, C. Fagiano, A. Doitrand, P. Lapeyronnie, V. Chiaruttini, F. E. Analysis, Meso-Scale Modeling of Damage in Textile Composites With Compacted and Nested Reinforcements, in: ECCM16 - 16TH EUROPEAN CONFERENCE ON COMPOSITE MATERIALS, Seville, Spain, 2014, pp. 22–26.

[10] S. Green, A. Long, B. El Said, S. Hallett, Numerical modelling of 3D woven preform deformations, Composite Structures 108 (2014) 747–756. doi:10.1016/j.compstruct.2013.10.015.
URL http://linkinghub.elsevier.com/retrieve/pii/S026382231300528X

[11] L. Wu, B. Gu, Fatigue behaviors of four-step three-dimensional braided composite material: a meso-scale approach computation, Textile Research Journal 84 (18) (2014) 1915–1930. doi:10.1177/0040517514540767.
URL http://trj.sagepub.com/cgi/doi/10.1177/0040517514540767

[12] L. Jin, B. C. Jin, N. Kar, S. Nutt, B. Sun, B. Gu, Tension-tension fatigue behavior of layer-to-layer 3-D angle-interlock woven composites, Materials Chemistry and Physics 140 (1) (2013) 183–190. doi:10.1016/j.matchemphys.2013.03.020.
URL http://dx.doi.org/10.1016/j.matchemphys.2013.03.020

[13] G. Yang, B. Sun, B. Gu, Large-scale finite element analysis of a 3D angle-interlock woven composite undergoing low-cyclic three-point bending fatigue, Journal of the Textile Institute 105 (3) (2014) 275–293. doi:10.1080/00405000.2013.836785.
URL http://www.tandfonline.com/doi/abs/10.1080/00405000.2013.836785

[14] Pyrofil Department, Typical Properties of Carbon Fiber, Tech. rep., Mitsubishi Corporation formerly named Mitsubishi Rayon Co. Ltd., Tokyo (2013).
URL www.mrc.co.jp

[15] Pyrofil Department, Mechanical Properties of PYROFIL Unidirectional Composite, Tech. rep., Mitsubishi Co. formerly named Mitsubishi Rayon Co. Ltd., Tokyo, Japan (2013).

[16] H. Miyagawa, T. Mase, C. Sato, E. Drown, L. T. Drzal, K. Ikegami, Comparison of experimental and theoretical transverse elastic modulus of carbon fibers, Carbon 44 (10) (2006) 2002–2008. doi:10.1016/j.carbon.2006.01.026.

[17] D. Ségur, Y. Guillet, B. Audoin, Intrinsic geometric scattering probed by picosecond optoacoustics in a cylindrical cavity: Application to acoustic and optical characterizations of a single micron carbon fiber, Applied Physics Letters 97 (3) (2010) 031901. doi:10.1063/1.3464563.
URL http://aip.scitation.org/doi/10.1063/1.3464563

[18] D. Mounier, C. Poilâne, C. Bûcher, P. Picart, Evaluation of transverse elastic properties of fibers used in composite materials by laser resonant ultrasound spectroscopy Evaluation of transverse elastic properties of fibers used in composite materials by laser resonant ultrasound spec- troscopy. Soci, Acoustics.
URL https://hal.archives-ouvertes.fr/hal-00811303

[19] R. Maurin, P. Davies, N. Baral, C. Baley, Transverse Properties of Carbon Fibres by Nano-Indentation and Micro-mechanics, Applied Composite Materials 15 (2) (2008) 61–73. doi:10.1007/s10443-008-9057-3.
URL http://dx.doi.org/10.1007/s10443-008-9057-3http://www.springerlink.comhttp://www.ifremer.fr/docelec/

[20] L. Kobets, I. Deev, Carbon fibres: structure and mechanical properties, Composites Science and Technology 57 (12) (1998) 1571–1580. doi:10.1016/S0266-3538(97)00088-2.
URL http://linkinghub.elsevier.com/retrieve/pii/S0266353897000882

[21] P. Soden, M. Hinton, A. Kaddour, Lamina properties, lay-up configurations and loading conditions for a range of fibre-reinforced composite laminates, Composites Science and Technology 58 (7) (1998) 1011–1022. doi:http://dx.doi.org/10.1016/S0266-3538(98)00078-5.
URL http://www.sciencedirect.com/science/article/pii/S0266353898000785

[22] R. P. Tavares, A. R. Melro, M. A. Bessa, A. Turon, W. K. Liu, P. P. Camanho, Mechanics of hybrid polymer composites: analytical and computational study, Computational Mechanics 57 (3) (2016) 405–421. doi:10.1007/s00466-015-1252-0.
URL http://link.springer.com/10.1007/s00466-015-1252-0

[23] J. Zhi, L. Zhao, J. Zhang, Z. Liu, A Numerical Method for Simulating the Microscopic Damage Evolution in Composites Under Uniaxial Transverse Tension, Applied Composite Materials 23 (3) (2016) 255–269. doi:10.1007/s10443-015-9459-y.
URL http://link.springer.com/10.1007/s10443-015-9459-y

[24] W. V. Liebig, C. Viets, K. Schulte, B. Fiedler, Influence of voids on the compressive failure behaviour of fibre-reinforced composites, Composites Science and Technology 117 (2015) 225–233. doi:10.1016/j.compscitech.2015.06.020.
URL http://linkinghub.elsevier.com/retrieve/pii/S0266353815300294

[25] M. Pathan, V. Tagarielli, S. Patsias, P. Baiz-Villafranca, A new algorithm to generate representative volume elements of composites with cylindrical or spherical fillers, Composites Part B: Engineering 110 (2017) 267–278. doi:10.1016/j.compositesb.2016.10.078.
URL http://www.sciencedirect.com/science/article/pii/S1359836816313725

[26] S. B. Clay, S. P. Engelstad, Benchmarking of composite progressive damage analysis methods: The background-doi:10.1177/0021998316672520.
URL http://journals.sagepub.com/doi/pdf/10.1177/0021998316672520

[27] S. P. Engelstad, S. B. Clay, Comparison of composite damage growth tools for static behavior of notched composite laminates, Journal of Composite Materials 51 (10) (2017) 1493–1524. doi:10.1177/0021998316675945.
URL http://journals.sagepub.com/doi/10.1177/0021998316675945

[28] R. W. Dalgarno, J. E. Action, D. H. Robbins, S. P. Engelstad, Failure simulations of open-hole and unnotched IM7/977-3 coupons subjected to quasi-static loading using Autodesk Helius PFA, Journal of Composite Materialsdoi:10.1177/0021998316653174.
URL http://jcm.sagepub.com/cgi/doi/10.1177/0021998316653174

[29] P. Naghipour, S. M. Arnold, E. J. Pineda, B. Stier, L. Hansen, B. A. Bednarcyk, A. M. Waas, Multiscale static analysis of notched and unnotched laminates using the generalized method of cells, Journal of Composite Materialsdoi:10.1177/0021998316651708.
URL http://jcm.sagepub.com/cgi/doi/10.1177/0021998316651708

[30] M. Kersemans, A. Martens, J. Degrieck, K. Van Den Abeele, S. Delrue, L. Pyl, F. Zastavnik, H. Sol, W. Van Paepegem, The Ultrasonic Polar Scan for Composite Characterization and Damage Assessment: Past, Present and Future, Applied Sciences 6 (2) (2016) 58. doi:10.3390/app6020058.
URL http://www.mdpi.com/2076-3417/6/2/58

[31] R. Kriz, W. Stinchcomb, Elastic moduli of transversely isotropic graphite fibers and their composites, Experimental Mechanics 19 (2) (1979) 41–49.

[32] W. Van Buskirk, S. Cowin, R. N. Ward, Ultrasonic measurement of orthotropic elastic constants of bovine femoral bone, Journal of Biomechanical Engineering 103 (2) (1981) 67–72.

[33] S. Fonteyn, Test result summary Static shear test [+45/-45]2s, Tech. rep., SIM M3Strength, Vrije Universiteit Brussel, Brussels (2015).

[34] A. Cernescu, Test result summary Static tensile test CEH [90], Tech. rep., SIM M3Strength, Vrije Universteit Brussel, Brussels (2017).

[35] S. Fonteyn, Test result summary Static tensile test CEH [0]4, Tech. rep., SIM M3Strength, Vrije Universiteit Brussel, Brussels (2015).

[36] ASTM, D3039/d3039m standard test method for tensile properties of polymer matrix composite materials, Annual Book of ASTM Standards (2014) 1–13doi:10.1520/D3039.
URL http://scholar.google.com/scholar?hl=en{\&}btnG=Search{\&}q=intitle:Standard+Test+Method+for+Tensile+Properties+of+Polymer+Matrix+Composite+Materials{\#}1

[37] ASTM, D3518 Standard Test Method for In-Plane Shear Response of Polymer Matrix Composite Materials by Tensile Test of a +45/-45 Laminate, Annual Book of ASTM Standards 94 (Reapproved) (2007) 1–7. doi:10.1520/D3518.

[38] K. Vallons, Test result summary Static tensile test CEH000, Tech. rep., SIM M3Strength, Katholieke Universiteit Leuven, Leuven, Belgium (2015).

[39] R. D. B. Sevenois, Test results summary Iosipescu shear test CEH000, Tech. rep., SIM M3Strength, Ghent University, Ghent, Belgium (2018).

[40] M. K. Ballard, W. R. McLendon, J. D. Whitcomb, The influence of microstructure randomness on prediction of fiber properties in composites, Journal of Composite Materials 48 (29) (2014) 3605–3620. doi:10.1177/0021998313511654.
URL http://dx.doi.org/10.1177/0021998313511654

[41] T. Mori, K. Tanaka, Average stress in matrix and average elastic energy of materials with misfitting inclusions, Acta Metallurgica 21 (5) (1973) 571–574. doi:10.1016/0001-6160(73)90064-3.
URL http://www.sciencedirect.com/science/article/pii/0001616073900643

[42] Y. Benveniste, A new approach to the application of Mori-Tanaka's theory in composite materials, Mechanics of materials 6 (2) (1987) 147–157.
URL http://www.sciencedirect.com/science/article/pii/0167663687900056

[43] G. Lielens, P. Pirotte, A. Couniot, F. Dupret, R. Keunings, Prediction of thermo-mechanical properties for compression moulded composites, Composites Part A: Applied Science and Manufacturing 29 (1) (1998) 63–70. doi:10.1016/S1359-835X(97)00039-0.
URL http://www.sciencedirect.com/science/article/pii/S1359835X97000390

[44] C. C. Chamis, Micromechanics strength theories. [for unidirectional composites], Tech. rep. (Jan. 1974).
URL https://ntrs.nasa.gov/search.jsp?R=19750040810

[45] B. D. Lubachevsky, F. H. Stillinger, Geometric properties of random disk packings, Journal of Statistical Physics 60 (5-6) (1990) 561–583. doi:10.1007/BF01025983.
URL http://link.springer.com/article/10.1007/BF01025983

[46] G. M. Knott, T. L. Jackson, J. Buckmaster, Random Packing of Heterogeneous Propellants, AIAA Journal 39 (4) (2001) 678–686. doi:10.2514/2.1361.
URL http://dx.doi.org/10.2514/2.1361

[47] J. W. Eaton, D. Bateman, S. Hauberg, R. Wehbring, GNU Octave version 4.2.0 manual: a high-level interactive language for numerical computations (2016).
URL http://www.gnu.org/software/octave/doc/interpreter

[48] Abaqus, User Documentation 2017, Dassault Systemes, RI, USA, 2017.

[49] D. Garoz, F. A. Gilabert, R. D. B. Sevenois, S. W. F. Spronk, W. Van Paepegem, Consistent Application of Periodic Boundary Conditions in Implicit and Explicit Finite Element Simulations of Damage, Composite Structures (2018) (Submitted).

[50] J. D. Eshelby, The Determination of the Elastic Field of an Ellipsoidal Inclusion, and Related Problems, Proceedings of the Royal Society of London. Series A. Mathematical and Physical Sciences 241 (1226) (1957) 376–396. doi:10.1098/rspa.1957.0133.
URL http://rspa.royalsocietypublishing.org/content/241/1226/376

[51] S. G. Abaimov, A. A. Khudyakova, S. V. Lomov, On the closed form expression of the MoriTanaka theory prediction for the engineering constants of a unidirectional fiber-reinforced ply, Composite Structures 142 (2016) 1–6. doi:10.1016/j.compstruct.2016.02.001.
URL http://www.sciencedirect.com/science/article/pii/S0263822316300216

[52] D. Blackketter, D. Upadhyaya, T. King, Micromechanics Prediction of the Transverse Tensile Strength of Carbon Fiber / Epoxy Composites : The Influence of the Matrix and Interface, Polymer Composites 14 (5) (1993) 437–446.

[53] H. Miyagawa, C. Sato, T. Mase, E. Drown, L. T. Drzal, K. Ikegami, Transverse elastic modulus of carbon fibers measured by Raman spectroscopy, Materials Science and Engineering A 412 (1-2) (2005) 88–92. doi:10.1016/j.msea.2005.08.037.

[54] G. Al Kassem, Micromechanical Material Models for Polymer Composites Through Advanced Numerical Simulation Techniques, Ph.D. thesis, Aachen University in Germany (2009).

[55] R. Younes, A. Hallal, F. Fardoun, F. Hajj, Comparative Review Study on Elastic Properties Modeling for Unidirectional Composite Materials, in: N. Hu (Ed.), Composites and Their Properties, InTech, 2012.
URL http://www.intechopen.com/books/composites-and-their-properties/comparative-review-study-on-elastic-properties-modeling-for-unidirectional-composite-materials

[56] C. C. Chamis, F. Abdi, M. Garg, L. Minnetyan, H. Baid, D. Huang, J. Housner, F. Talagani, Micromechanics-based progressive failure analysis prediction for WWFE-III composite coupon test cases, Journal of Composite Materials 47 (20-21) (2013) 2695–2712. doi:10.1177/0021998313499478.
URL https://doi.org/10.1177/0021998313499478

[57] S. Fonteyn, Test result summary Static Tensile Test CEH[#(45/-45)]4s, Tech. rep., SIM M3Strength, Vrije Universiteit Brussel, Brussels (2015).

[58] S. Fonteyn, Test result summary Static tensile test CEH[#(0/90)]4s, Tech. rep., SIM M3Strength, Vrije Universiteit Brussel, Brussels (2015).